Pancharatnam–Berry Phase Manipulating Metasurface for Visible Color Hologram Based on Low Loss Silver Thin Film

Sajid Choudhury, Urcan Guler, Amr Shaltout, Vladimir M. Shalaev, Alexander V. Kildishev, and Alexandra Boltasseva**

This study demonstrates visible color hologram using a plasmonic metasurface. The metasurface is fabricated by perforating nanoslits in a 50 nm thick monocrystalline silver film that is ultrasmooth and has ultralow loss compared to conventional polycrystalline silver films commonly used in plasmonics. The designed plasmonic hologram is the thinnest metasurface hologram operating in transmission mode to the best of our knowledge. Holograms of three individual component colors (red, green, and blue) are demonstrated in transmission mode, and a scheme for generating polychromatic hologram is illustrated. By adjusting the slit dimensions and orientation, the phase of a visible spectrum light can be controlled, paving the way to applications of ultracompact polychromatic plasmonic metasurfaces for advanced light manipulation.

1. Introduction

Recent advances in the area of metasurfaces[1–4] provided the opportunity to manipulate light at an ultracompact, subdiffraction scale. The concept of metasurfaces came from utilizing the generalized Snell's law.[1] Wavefronts of incoming light are modified by a metasurface by introducing abrupt phase jumps at the interface of a structure.[5] Bomzon et al. first proposed to use Pancharatnam–Berry phase optical elements for converting wavefronts of cylindrical beams.[6] They were later used for metasurfaces by Kang et al.,[7] which led to additional applications involving the Pancharatnam–Berry phase, such as ultrathin flat lenses,[8] focusing mirrors,[9] spin-dependent directional coupling,[10,11] spectroscopy,[12,13] polarization control,[14] and ultracompact tunable optical devices.[15] To get the properties of phase manipulation at a subwavelength scale, suitable material platforms are a necessity. Noble metals, as well as alternative materials, have been proposed for metasurface construction. Alternative materials such as transition metal nitrides and complex oxide such as transparent conducting oxides[16] have been also introduced for various plasmonic applications. For alternative material platforms, the primary focus is on low loss, tunability, fabrication compatibility for integrated platforms and high temperature applications.[17] Most reported alternative materials are dielectric or very weakly plasmonic in the blue region of the visible spectrum.[18] For visible frequencies metasurfaces, plasmonic noble metals, such as aluminum[19,20] and silver,[21] have been utilized so far. Noble metals, such as gold and silver, have inherent loss limitations for fully realizing the potentials of plasmonics.[22] While making thin films or nanostructures with silver, the grain-boundaries introduce additional loss in the material[23] and therefore, the full potential of the plasmonic noble metals cannot be utilized. Aluminum is lossy compared to silver in the visible spectrum. On the other hand, dielectric metasurfaces have been introduced with increased efficiency for optical metasurface applications,[24] but with thicknesses much larger than the optical wavelength in the corresponding material.

To prepare subwavelength optical elements for visible wavelengths operation, silver is the most suitable elemental material. Silver films grown on transparent substrates are typically polycrystalline. The grain boundaries in the film give rise to additional optical losses, which prohibits the full potential of silver as a plasmonic material from being realized. Silver films, free from grain boundaries, can significantly reduce the losses incurred in polycrystalline films and can therefore reduce the losses. In this paper, we use low loss ultrasmooth epitaxial silver films as the material platform to generate hologram. It has been demonstrated previously that silver (001) can be grown epitaxially on MgO (001) substrate with the help of epitaxial TiN layer.[25] Demonstrated silver films show lowest loss for silver grown on transparent substrate. Monochromatic holograms have been created at subwavelength scale using extreme light confinement of resonant plasmonic structures, such as V-antennas,[26] nanorods,[27] nanopillars,[28] and subwavelength gratings.[29] Principally, the combination of the three basic element colors, red, green, and blue, can be utilized to make a color image. Most plasmonic metals are dielectric or less plasmonic in the blue region. It is therefore difficult to produce a blue color component for multicolor holograms using a plasmonic metasurface. Color holograms have been generated

S. Choudhury, Dr. U Guler, Prof. V. M. Shalaev,
Prof. A. V. Kildishev, Prof. A. Boltasseva
School of Electrical and Computer Engineering
and Birck Nanotechnology Center
Purdue University
West Lafayette, IN 47907, USA
E-mail: kildisha@purdue.edu; aeb@purdue.edu
Dr. A. Shaltout
Stanford University
Stanford, CA 94305, USA
The ORCID identification number(s) for the author(s) of this article can be found under http://dx.doi.org/10.1002/adom.201700196.

DOI: 10.1002/adom.201700196

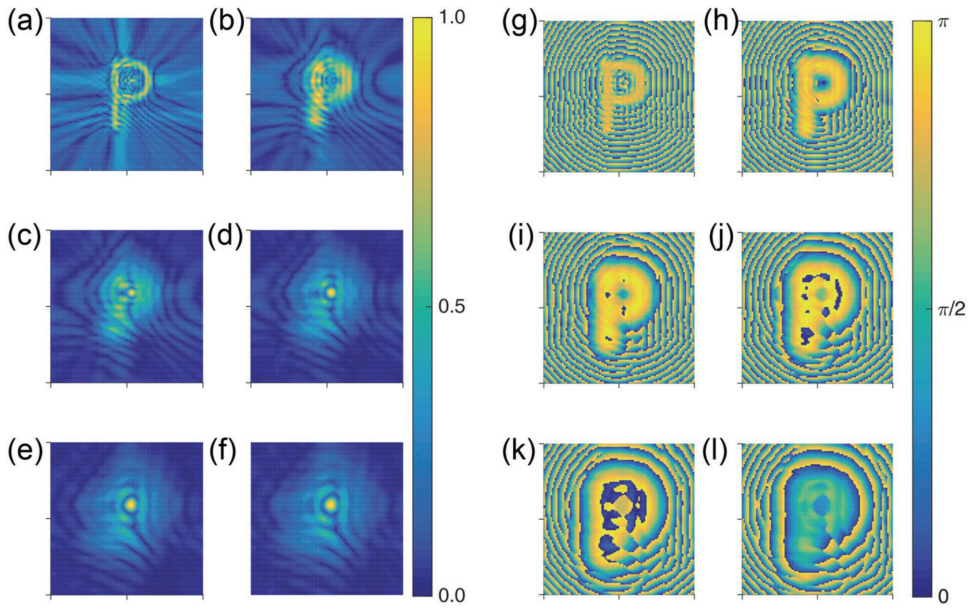

Figure 1. a–f) Amplitude and g–l) phase of the wavefronts from a letter P with dimension of 10 µm. The total length of each axis of the images is 20 µm (–10 to 10 µm shown in axis ticks). The image is assumed to be comprised of point sources and the wavefront is calculated at distances away from the image plane. The distance of the wavefront a,g) 1 µm, b,h) 3 µm, c,i) 5 µm, d,j) 7 µm, e,k) 9 µm, and f,l) 10 µm.

with white light excitation of surface plasmons in diffraction gratings.[30,31] Orthogonal polarizations with different resonant structures have also been used to produce dual-color holograms in reflection mode.[32] Recently, multicolor holograms have been demonstrated with metal–insulator–metal gap plasmonic structures,[19] metallic slits,[33] and rotated dielectric nanobars.[34,35]

This paper introduces monocrystalline silver grown on a transparent substrate as a material platform for plasmonic metasurfaces. As a demonstration, in this paper, we experimentally realize holograms in transmission mode. This is a first demonstration of a ultrasmooth, low-loss silver-based metasurface. All three component colors required for a multicolor hologram are demonstrated experimentally. The designed Pancharatnam–Berry phase manipulating metasurface can modify the phase of an incoming light to produce a color hologram at a virtual imaging plane. The paper also illustrates a scheme to create multicolor holograms in the visible range with all color components present. The demonstrated experimental scheme is achieved with the help of an ultrasmooth 50 nm thick silver film, that has best demonstrated optical property grown on a transparent substrate. The metasurface design scheme paves the way to developing ultracompact polychromatic optical elements at visible wavelengths.

2. Designing

A hologram can be generated by controlling the amplitude and phase of an incoming light. As per Huygen's principle, every point in a wavefront acts as secondary sources. So, if the amplitude and phase of each point of a wavefront of an image is known, the image can be constructed by inverse design. This can be done by placing a point source at each point of the wavefront with the same amplitude and phase as the original incident wave. The electromagnetic field emitted from a point source can be obtained through the Green function representation[36]

$$G = -\frac{1}{4\pi|\mathbf{r_d} - \mathbf{r_s}|}\exp\left(i\frac{2\pi}{\lambda}|\mathbf{r_d} - \mathbf{r_s}|\right)$$

where $|\mathbf{r_d} - \mathbf{r_s}|$ gives the distance between a particular point in space and the source point. Hence, the amplitude and phase of the wavefront, $A(\boldsymbol{r})\exp(i\Phi(\boldsymbol{r}))$ at a distance away from the point sources can be calculated by summing over the complex intensities of the point sources.

If we take the inverse problem and assume point sources with amplitude $A(\boldsymbol{r})$ and phase $\Phi(\boldsymbol{r})$ placed at discrete points in space, we can reconstruct the original images. To create a color hologram, the amplitude and phase of each color components have to be calculated at the wavefront. While reconstructing the image, quantization noise would be present due to a finite number of sources at the wavefront plane. This can be minimized by placing the sources as compact as possible. To illustrate the amplitude and phase profile of the wavefront, we consider an image of the letter P with length 10 µm, and calculate the amplitude and phase points at various distances. **Figure 1**a–f shows the amplitude profile and Figure 1g–l shows the phase profiles at different distances from the image plane at $\lambda = 676$ nm. For each set of amplitude and phases, the complete image can be reconstructed at the same distance with the availability of point sources of the same amplitude and phase. Now, to generate a color hologram at an image plane, the amplitude and phase of each color components should be calculated at the wavefront plane. Accordingly, if the point sources are introduced with same amplitude and phase as the colors at the wavefront plane, it is possible to reconstruct the initial image at the virtual image plane.

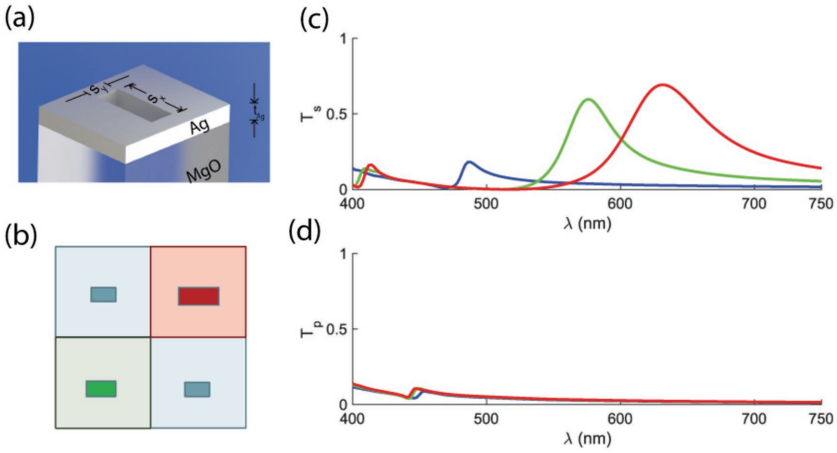

Figure 2. a) 3D Illustration of a unit cell for a color. b) Proposed supercell containing unit cells of each color. Blue, green, and red colored rectangle represent their respective slits with desired resonant frequency c) s-polarized and d) p-polarized transmission coefficient simulated for three different slit lengths, blue, green, and red represent three different lengths of slit.

In this work, we used a nanoslit-based metasurface. The transmission peak of a complimentary nanoslit antenna can be tuned by adjusting the antenna length. **Figure 2**a shows a unit cell for a single color, which consists of an MgO substrate with silver. The center part is patterned with a nanoslit, where s_x and s_y represent the dimensions of the slit. The slit dimensions are optimized in such a manner that it propagates minimum light for p-polarized light and maximum light for s-polarized light. The three-color components, red, green and blue, are represented by 676, 520, and 488 nm wavelength, respectively. For a film thickness of t_{Ag} = 50 nm and s_x = 30 nm, the dimensions of the slits representing different colors were s_y = 40 nm for blue, s_y = 60 nm for green, and s_y = 110 nm for red color. Since the blue slit resonance is weaker compared to the green and red slit resonances, twice the number of blue slits are used to represent each color point. Figure 2b shows the illustration of a complete supercell representing one complex amplitude and phase of a point with three colors. The red, green, and blue colors represent the position of red, green, and blue unit cells within the supercell. Figure 2c,d shows the p-polarized and s-polarized transmission coefficients of individual slits. Each unit cell shows the transmission resonance at the designed wavelength for s-polarized and minimum p-polarized transmission. The amplitude obtained by each antenna is fixed, while the phase can be adjusted by rotating the antennas. For our color hologram-generating scheme, we should use a binary amplitude modulation scheme and arbitrary phase modulation scheme. In practice, the phase modulation of the angles is limited by the fabrication tolerance of the structures. Rotating each of the apertures causes each antenna to introduce a geometric phase to the propagating light beam.

3. Result and Discussion

We use epitaxial silver thin films grown on MgO substrate to fabricate the metasurface. The thin film is characterized with a VASE ellipsometer to obtain the optical constants. **Figure 3**a,b shows the real and imaginary part of the electric permittivity of the silver film grown on MgO and it is compared to recently published works[37,38] on epitaxial silver thin films grown on silicon-111 and reported thicker silver films.[39,40] Our silver film shows lowest loss compared to other silver films of equivalent

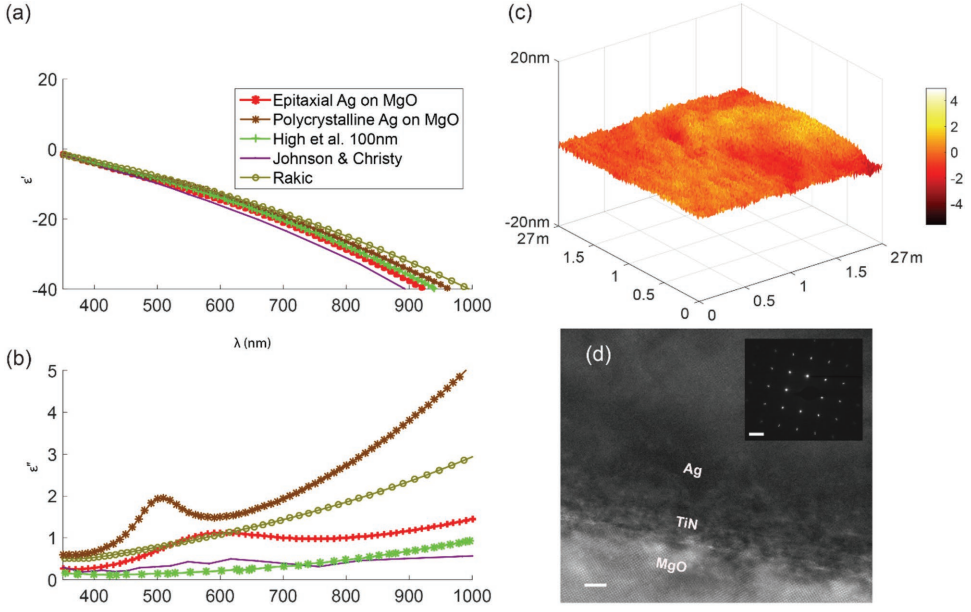

Figure 3. Optical properties and AFM image of the silver on MgO. a) Real and b) imaginary part of permittivity of the silver film. c) AFM measurement of surface roughness profile of the silver film. d) TEM measurement of the silver film. Scale bars represent 5 nm.

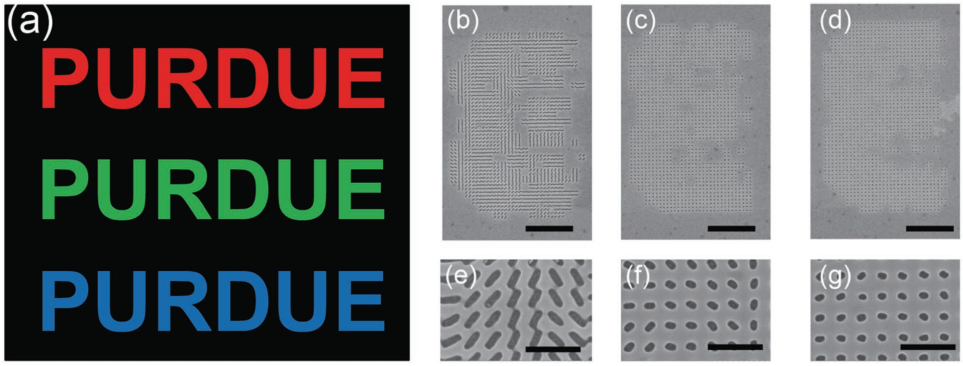

Figure 4. a) Input image for the fabricated metasurface. b–g) SEM Images of the fabricated metasurface structures. b–d) Scale bar is 2.5 μm. e–g) Scale bar is 500 nm. Panels b–e) shows antennas for red color, c,f) shows antennas for green color, and d,g) shows antennas for blue color.

thickness, grown on transparent substrate. Comparing to the recent works, our film shows comparable loss at blue wavelengths while losses peak at red wavelengths. The thickness of the grown film is only 50 nm and is quite suitable for producing a metasurface to manipulate light. Figure 3c shows the atomic force microscopy (AFM) measurement of the silver surface. The grown film is ultrasmooth, with an RMS roughness R_a of 0.318 nm. Figure 3d shows the TEM measurement of the film (FFT shown in the inset). From the TEM analysis, it is evident that both the silver and TiN thin films are epitaxial. (see Supporting Information for a more detailed characterization of the silver film.)

To generate the three component colors with the metasurface, a sample image with PURDUE written with red, green, and blue color was taken. **Figure 4**a shows the input bitmap image. Assuming point sources as the bitmap pixels, the amplitude and phases of the wavefront at 5 μm distance are calculated for a periodicity of 360 nm. The field of exposure of the FIB for restricts accurate reproduction of the slits, we are limited by the field of exposure of the FIB. The total length of the pattern is limited to 10 μm. Therefore, the total area of the metasurface was also limited. To illustrate the concept that three component colors could be generated, unit cells consisting of only individual colors red, green and blue has been considered. Angular resolution was also limited by the finite grid of the FIB (3 nm), and determined by the ability to resolve two separate angles through rotation of the slit pattern in the finite grid. The average angular resolutions are calculated to be 2.4172 ± 1.1883°, 4.9513 ± 2.1996°, and 7.4687 ± 3.1078° for red, green, and blue slits, respectively. The simulated transmission in Figure 2c,d could not be measured experimentally due to the size constraint of the pattern. The amplitude is modulated with a binary amplitude modulation with a threshold of 33%. Thresholding amplitude is a good approximation to represent the wavefront of the image. Each point in the wavefront is represented with the unit consisting of the designed nanoslits rotated as per the geometric phase of the wavefront. The slits were patterned onto the silver film with FEI Ga-ion focused ion beam. It is known that Ga-ion FIB causes contamination to silver films, so some degradation of their performance is expected from the metasurface. In addition, due to the smaller feature sizes of the slits, it was difficult to do e-beam lithography and get proper features at such a small scale. Moreover, the FIB writing limits the total dimensions of the pattern area to 10 μm × 10 μm. Due to these pattern area constrains, only the simulated transmission spectrum from Figure 2 was used to design the metasurface.

Due to this pattern size limitation, only the simulated transmission spectrum from Figure 2 was used to design the metasurface. Figure 4b–g shows an SEM image of the fabricated structures for red, green, and blue portions of the image.

Figure 5a shows the experimental setup for the hologram observation. An Ar–Kr laser light source is circularly polarized and is illuminated on the sample from the transmission side. The microscope stage is moved in precision to 5 μm above the surface of the film to observe the holographic images shown in Figure 5b, which successfully resolves the three-color components. The observed blue color is more red shifted. This could be attributed to the fabricated apertures being larger than the designed nanoslits for blue color. To illustrate the formation of the hologram at the focal plane, we focused the surface of the patterned silver film with the microscope and gradually rotated the focusing knob to translate the stage in z direction at the micrometer scale. **Figure 6** shows the camera image for each focusing plane. The hologram image is observed to be sharpest at the designed distance of 5 μm. The camera software causes

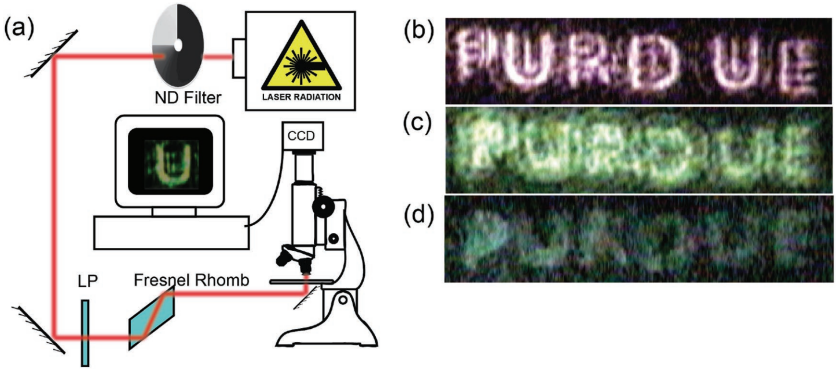

Figure 5. a) Experimental setup. Final hologram image captured through CCD camera for b) red, c) green, and d) blue hologram.

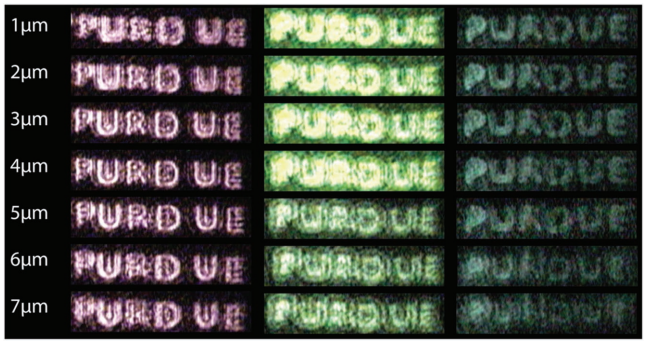

Figure 6. Hologram observation by change of focus of the microscope. Left column shows the distance of the focal plane of the microscope set from the surface of the silver film. Each row corresponds to the focal plane for the hologram color.

automatic correction to the contrast and brightness of individual color components. This caused slight variation of image color in the final output. Blurring of the images can be attributed to the finite grid size, and angular resolution discontinuity.

4. Conclusions

A hologram generated by a plasmonic metasurface fabricated on ultrasmooth low-loss silver film is demonstrated experimentally. The total thickness of the silver layer is 50 nm, and this is the thinnest metasurface hologram demonstrated in transmission mode. The metasurface is developed by manipulating the Pancharatnam– Berry phase of incoming light. The low-loss silver-based metasurface can work in transmission mode and manipulate light at ultrathin thickness. The designed nanoapertures work well in the visible region and can produce a three-color image at a virtual imaging plane. The fabrication procedure developed can be utilized in future applications of plasmonic metasurfaces such as vortex beam generation, polarization conversion, biosensing, and paves the way to new applications of polychromatic plasmonic metasurfaces in the visible regime.

5. Experimental Section

Fabrication: A 4 nm thick TiN layer, which also served as a seed layer for the epitaxial growth, was used underneath the silver film to improve film stability. The thin TiN layer was deposited at 800 °C and 200 W power using a Ti target under 10^{-5} mTorr. A nitrogen and argon flow of 8:2 sccm was maintained while depositing the TiN film. Silver was deposited with a silver target with 50 W power. The nanoslits were fabricated using a FEI Nova-200 DualBeam Ga-ion FIB. The slits were observed using a Hitachi S-4800 FE-SEM. Final patterns were observed using CSC-790 NTSC CCD Camera.

Experiment: Collimated beam from an Ar–Kr laser was used as illumination light source. Slit position corresponding to 483, 530, and 647 nm was used for red green and blue light sources, respectively. For the white light source, a fiber-coupled NKT-Super K laser source was used. A Raman spectroscopic setup is modified for observing the hologram. Laser illumination was attenuated with a variable neutral density filter and passed through a broadband linear polarizer. A Fresnel Rhomb was used to convert the linear polarized beam into circular polarized beam and the sample was illuminated by the output from the Fresnel Rhomb from the bottom. The hologram was observed by focusing the microscope at 10 μm above the sample plane using a 50× objective and observing the hologram using a CCD camera.

Supporting Information

Supporting Information is available from the Wiley Online Library or from the author.

Acknowledgements

This work was supported by U.S. Army Research Office grant 63133-PH (W911NF-13-1-0226) and the Air Force Office of Scientific Research MURI grant (FA9550-14-1-0389). Authors gratefully acknowledge S. Rouvimon and T.A. Orlova for help with TEM analysis and A. Dutta for help with XRD and C. DeVault, D. Shah for helping with proofreading the manuscript.

Conflict of Interest

The authors declare no conflict of interest.

Keywords

holograms, metasurfaces, Pancharatnam–Berry phases, plasmonics

Received: March 1, 2017
Published online: April 24, 2017

[1] N. Yu, P. Genevet, M. A. Kats, F. Aieta, J.-P. Tetienne, F. Capasso, Z. Gaburro, *Science* **2011**, *334*, 333.
[2] D. Veksler, E. Maguid, N. Shitrit, D. Ozeri, V. Kleiner, E. Hasman, *ACS Photonics* **2015**, *2*, 661.
[3] D. Lin, P. Fan, E. Hasman, M. L. Brongersma, *Science* **2014**, *345*, 298.
[4] A. V. Kildishev, A. Boltasseva, V. M. Shalaev, *Science* **2013**, *339*, 1289.
[5] N. Yu, F. Capasso, *Nat. Mater.* **2014**, *13*, 139.
[6] Z. Bomzon, G. Biener, V. Kleiner, E. Hasman, *Opt. Lett.* **2002**, *27*, 1141.
[7] M. Kang, T. Feng, H.-T. Wang, J. Li, *Opt. Express* **2012**, *20*, 15882.
[8] F. Aieta, P. Genevet, M. A. Kats, N. Yu, R. Blanchard, Z. Gaburro, F. Capasso, *Nano Lett.* **2012**, *12*, 4932.
[9] A. Pors, M. G. Nielsen, R. L. Eriksen, S. I. Bozhevolnyi, *Nano Lett.* **2013**, *13*, 829.
[10] S. Xiao, F. Zhong, H. Liu, S. Zhu, J. Li, *Nat. Commun.* **2015**, *6*, 8360.
[11] J. Lin, J. P. B. Mueller, Q. Wang, G. Yuan, N. Antoniou, X.-C. Yuan, F. Capasso, *Science* **2013**, *340*, 331.
[12] M. Khorasaninejad, W. T. Chen, J. Oh, F. Capasso, *Nano Lett.* **2016**, *16*, 3732.
[13] A. Shaltout, J. Liu, A. Kildishev, V. Shalaev, *Optica* **2015**, *2*, 860.
[14] Y. Zhao, A. Alù, *Phys. Rev. B* **2011**, *84*, 205428.
[15] N. Meinzer, W. L. Barnes, I. R. Hooper, *Nat. Photonics* **2014**, *8*, 889.
[16] G. V. Naik, J. Kim, A. Boltasseva, *Opt. Mater. Express* **2011**, *1*, 1090.
[17] W. Li, U. Guler, N. Kinsey, G. V. Naik, A. Boltasseva, J. Guan, V. M. Shalaev, A. V. Kildishev, *Adv. Mater.* **2014**, *26*, 7959.
[18] P. R. West, S. Ishii, G. V. Naik, N. K. Emani, V. M. Shalaev, A. Boltasseva, *Laser Photonics Rev.* **2010**, *4*, 795.
[19] Y. W. Huang, W. T. Chen, W. Y. Tsai, P. C. Wu, C. M. Wang, G. Sun, D. P. Tsai, *Nano Lett.* **2015**, *15*, 3122.

[20] W. Wan, J. Gao, X. Yang, *ACS Nano* **2016**, *10*, 10671.
[21] G. M. Akselrod, J. Huang, T. B. Hoang, P. T. Bowen, L. Su, D. R. Smith, M. H. Mikkelsen, *Adv. Mater.* **2015**, *27*, 8028.
[22] J. B. Khurgin, A. Boltasseva, *MRS Bull.* **2012**, *37*, 768.
[23] V. P. Drachev, U. K. Chettiar, A. V. Kildishev, H.-K. Yuan, W. Cai, V. M. Shalaev, *Opt. Express* **2008**, *16*, 1186.
[24] A. I. Kuznetsov, A. E. Miroshnichenko, M. L. Brongersma, Y. S. Kivshar, B. Luk'yanchuk, *Science* **2016**, *354*, 6314.
[25] J. S. Chawla, D. Gall, *J. Appl. Phys.* **2012**, *111*, 43708.
[26] X. Ni, A. V Kildishev, V. M. Shalaev, *Nat. Commun.* **2013**, *4*, 2807.
[27] L. Huang, X. Chen, H. Mühlenbernd, H. Zhang, S. Chen, B. Bai, Q. Tan, G. Jin, K.-W. Cheah, C.-W. Qiu, J. Li, T. Zentgraf, S. Zhang, *Nat. Commun.* **2013**, *4*, 2808.
[28] W. Zhao, H. Jiang, B. Liu, J. Song, Y. Jiang, C. Tang, J. Li, *Sci. Rep.* **2016**, *6*, 30613.
[29] J. Lin, P. Genevet, M. A. Kats, N. Antoniou, F. Capasso, *Nano Lett.* **2013**, *13*, 4269.
[30] M. Ozaki, J. Kato, S. Kawata, *Science* **2011**, *332*, 218.
[31] M. Khorasaninejad, F. Capasso, *Nano Lett.* **2015**, *15*, 6709.
[32] W. T. Chen, K. Y. Yang, C. M. Wang, Y. W. Huang, G. Sun, I. Da Chiang, C. Y. Liao, W. L. Hsu, H. T. Lin, S. Sun, L. Zhou, A. Q. Liu, D. P. Tsai, *Nano Lett.* **2014**, *14*, 225.
[33] X. Li, L. Chen, Y. Li, X. Zhang, M. Pu, Z. Zhao, X. Ma, Y. Wang, M. Hong, X. Luo, *Sci. Adv.* **2016**, *2*, e1601102.
[34] W. Zhao, B. Liu, H. Jiang, J. Song, Y. Pei, Y. Jiang, *Opt. Lett.* **2016**, *41*, 147.
[35] B. Wang, F. Dong, Q.-T. Li, D. Yang, C. Sun, J. Chen, Z. Song, L. Xu, W. Chu, Y.-F. Xiao, Q. Gong, Y. Li, *Nano Lett.* **2016**, *16*, 5235.
[36] X. Ni, A. V. Kildishev, V. M. Shalaev, *Nat. Commun.* **2013**, *4*, 2807.
[37] Y. Wu, C. Zhang, N. M. Estakhri, Y. Zhao, J. Kim, M. Zhang, X. X. Liu, G. K. Pribil, A. Alù, C. K. Shih, X. Li, *Adv. Mater.* **2014**, *26*, 6106.
[38] A. A. High, R. C. Devlin, A. Dibos, M. Polking, D. S. Wild, J. Perczel, N. P. De Leon, M. D. Lukin, H. Park, *Nature* **2015**, *522*, 192.
[39] P. B. Johnson, R. W. Christy, *Phys. Rev. B* **1972**, *6*, 4370.
[40] E. D. Palik, *Proc. Natl. Acad. Sci. USA* **1991**, *2*, 1096.

